3018–3030 *Nucleic Acids Research, 2012, Vol. 40, No. 7* *Published online 9 December 2011*
doi:10.1093/nar/gkr1113

Structural activation of the transcriptional repressor EthR from *Mycobacterium tuberculosis* by single amino acid change mimicking natural and synthetic ligands

Xavier Carette[1,2,3,4], Nicolas Blondiaux[1,2,3,4], Eve Willery[1,2,3,4], Sylviane Hoos[5,6], Nathalie Lecat-Guillet[1,2,3,4], Zoé Lens[2,7], Alexandre Wohlkönig[8], René Wintjens[9], Sameh H. Soror[8], Frédéric Frénois[2], Bertrand Dirié[2,10,11], Vincent Villeret[2,7], Patrick England[5,6], Guy Lippens[12], Benoit Deprez[2,10,11], Camille Locht[1,2,3,4], Nicolas Willand[2,10,11] and Alain R. Baulard[1,2,3,4,*]

[1]Center for Infection and Immunity of Lille, F-59019 Lille, [2]Univ Lille Nord de France, F-59000 Lille, [3]CNRS, UMR8204, F-59021 Lille, [4]INSERM, U1019, F-59019 Lille, [5]Institut Pasteur, Plate-forme de Biophysique des Macromolécules et de leurs Interactions, F-75724 Paris, [6]CNRS URA 2185, F-75724 Paris, [7]IRI, USR3078 CNRS, F-59658 Villeneuve d'Ascq, France, [8]VIB, Department of Structural Biology, [9]Faculté de Pharmacie, Université Libre de Bruxelles, Bruxelles, Belgium, [10]Biostructures and Drug Discovery, INSERM U761, Lille F-59000, [11]Institut Pasteur de Lille, Lille F-59019 and [12]CNRS, UMR 8576, F-59655 Villeneuve d'Ascq, France

Received February 17, 2011; Revised November 5, 2011; Accepted November 7, 2011

ABSTRACT

Ethionamide is an antituberculous drug for the treatment of multidrug-resistant *Mycobacterium tuberculosis*. This antibiotic requires activation by the monooxygenase EthA to exert its activity. Production of EthA is controlled by the transcriptional repressor EthR, a member of the TetR family. The sensitivity of *M. tuberculosis* to ethionamide can be artificially enhanced using synthetic ligands of EthR that allosterically inactivate its DNA-binding activity. Comparison of several structures of EthR co-crystallized with various ligands suggested that the structural reorganization of EthR resulting in its inactivation is controlled by a limited portion of the ligand-binding-pocket. *In silico* simulation predicted that mutation G106W may mimic ligands. X-ray crystallography of variant G106W indeed revealed a protein structurally similar to ligand-bound EthR. Surface plasmon resonance experiments established that this variant is unable to bind DNA, while thermal shift studies demonstrated that mutation G106W stabilizes EthR as strongly as ligands. Proton NMR of the methyl regions showed a lesser contribution of exchange broadening upon ligand binding, and the same quenched dynamics was observed in apo-variant G106W. Altogether, we here show that the area surrounding Gly106 constitutes the molecular switch involved in the conformational reorganization of EthR. These results also shed light on the mechanistic of ligand-induced allosterism controlling the DNA binding properties of TetR family repressors.

INTRODUCTION

Tuberculosis (TB) is the leading cause of death due to a bacterial infection and accounts for 2.5% of all preventable deaths globally. The major obstacle to the global control of tuberculosis is the difficulties to detect and cure enough cases to interrupt transmission (1). Moreover, development and transmission of *Mycobacterium tuberculosis* strains resistant to multiple antibiotics (MDR) are emerging problems of major

*To whom correspondence should be addressed. Tel: +33 320 871153; Fax: +33 320 871157; Email: alain.baulard@pasteur-lille.fr
Correspondence may also be addressed to Nicolas Willand. Tel: +33 320 964 991; Fax: +33 320 964 709; Email: nicolas.willand@univ-lille2.fr
Present addresses:
Frédéric Frénois, Inserm U837, F-59045 Lille France.
Bertrand Dirié, LMC, University of Antwerpen, B-2000 Antwerpen, Belgium.

importance to public health with mortality rates much higher than the one associated to drug-sensitive TB. MDR-TB patients require specialized antibiotics often associated to serious side effects, which weaken the observance and lead to treatment failure. In addition, patients infected with MDR-TB remain infectious for longer than patients infected with drug-sensitive strains. Multiparametric strategies are needed in order to break this vicious circle. Identification of new molecules active against yet unexploited targets is obviously essential and recent efforts have led to the discovery of such promising compounds. It is, however, likely that these new antibiotics will need to be used in combination with drugs of the current regimens (2). Thus, improvement of the existing treatments should be considered with the aim of reducing their toxicity, thus favoring observance and eventually boosting treatment success (3).

In previous studies, we and others showed that sensitivity of *M. tuberculosis* to pro-antibiotics such as isoniazid (4), pyrazinamide (5), ethionamide (ETH) (6,7) and thiacetazone (8) is limited by the suboptimal activity of mycobacterial enzymes responsible for their bioactivation. In particular, ETH needs to be bioactivated by the mycobacterial monooxygenase EthA to acquire its antibacterial properties. The production of EthA is controlled by EthR, a mycobacterial transcriptional repressor of the TetR family. Deregulation of the production of EthA obtained experimentally by genetic inactivation of the EthR coding gene demonstrated that this repressor is responsible for a significant level of natural resistance of *M. tuberculosis* to ETH (6). Studies of the mechanisms of repression of *ethA* by EthR revealed that this repressor of the TetR family binds DNA as four dimers overlapping as much as 55 bp located upstream the *ethA* open reading frame (9), thus congesting the transcription initiation site of this gene.

Equilibrium between repression and derepression of genes regulated by TetR-type of repressors has been mainly shown to be controlled by ligands (10), with notable exceptions such as AmtR, which is controlled by protein complex formation (11). At critical concentrations, these ligands induce conformational modifications of the repressors, eventually transmitted to characteristic mirrored DNA binding motifs, leading to the release of the protein from DNA. Two independent crystal structures of EthR confirmed typical structurally conserved helix-turn-helix (HTH) DNA binding motifs within an N-terminal three-helix bundle and a larger C-terminal helical domain of dimerization. More importantly, both structures revealed fortuitous and highly different ligands in the repressor. The first structure was characterized by the presence of hexadecyl octanoate in the core domain of each monomer of EthR (PDB: 1U9N), thus revealing the long linear ligand binding pocket of the repressor (3). The other structure revealed the presence of two 6-membered cyclic molecules, possibly dioxane, in the ligand binding pocket of each monomer (PDB: 1T56) (12). By comparison with other members of the TetR family, the presence of either hexadecyl-octanoate or dioxane is translated in structural modifications of the DNA binding heads which keep them in a configuration incompatible with DNA binding (13).

With the objective of increasing the sensitivity of *M. tuberculosis* to ETH, we recently designed synthetic ligands to specifically bind the ligand binding site of EthR and we demonstrated their capacity to inhibit EthR–DNA interactions (14). Bacteria treated with such EthR-inhibitors showed a substantial increase of *ethA* mRNA production which was then correlated to a 20-time increase of sensitivity to ETH. Finally, one ligand was able to triple the efficiency of ETH on a TB-infected mice model. Fortuitous and synthetic ligands of EthR identified so far interact with various sections of the ligand binding pocket of the regulator. Interestingly, crystal structures revealed that while the pocket of EthR is able to accept very long ligands (3), smaller molecules with occupancy limited to the upper part of the pocket are sufficient to induce conformational changes impairing the repressor function of the protein (12,14–16).

In the present study, we have compared all these structures to delineate the common structural region of EthR involved in the interaction with different ligands. This allowed us to propose a minimal region of interaction between EthR and ligand necessary for inducing the structural movements of the DNA binding motifs. *In silico* simulations of amino acid replacement followed by experimental validation confirmed the predominant role of the G106 region for ligand recognition process and for the initiation of the structural reorganization of the regulator. These results will help drive the development of improved synthetic EthR inhibitors towards reduced ETH dosage treatment. Importantly, these data contribute to the basic understanding of the intramolecular communication between the ligand binding domain and the DNA binding domain in TetR type repressors.

MATERIALS AND METHODS

Construction of pET15b-ethR-G106W

A first PCR product was obtained by amplification using *M. tuberculosis* H37Rv chromosomic DNA as template and oligonucleotides O-275 (5′AGGACCGTCCGCTGG CCGATA-3′) and O-276 (5′AACACGTTGAT**CCA**GGT GCGCCACA-3′) as primers, thus introducing a point mutation at codon 106 of *ethR* (underlined in oligonucleotide O-276), resulting in the replacement of Glycin 106 by a tryptophane. This 216-bp fragment was used as a 5′ primer in association with oligonucleotide O-278 (5′GCTTCCTTTCGGGCTTTGTTAGCAG-3′) to amplify a 594-bp fragment, which was subsequently inserted in PCRII-Topo (Invitrogen) to generate pCRIIethRG106W. The 275-bp SalI–SalI fragment of pET15b-ethR (9) was then exchanged for the equivalent fragment of pCRIIethRG106W to produce pET15b-ethR-G106W. The orientation of the fragment was checked by restriction and the DNA sequence was confirmed by sequencing of the entire ORF.

Production and purification of EthR and variant $EthR_{G106W}$

N-terminally hexa-histidine-tagged EthR WT or $EthR_{G106W}$ were produced in *Escherichia coli* C41 using the protein expression plasmids pET15b-ethR and pET15b-ethR-G106W, respectively, as previously described (9). Bacteria were grown at 37°C in 100 ml LB broth to an OD_{600} nm of 0.6–0.7. Isopropylthiogalactoside (IPTG) was then added to a final concentration of 1 mM and the culture was grown for 3 h at 37°C. The cells were harvested by centrifugation at 12 000*g* at 4°C, resuspended in 10 ml of lysis buffer (50 mM Tris/HCl, 300 mM NaCl, pH 7.5, 10 mM imidazole) and lysed by two passages at 6.2 MPa through a French Press cell. After centrifugation (20 000*g*, 25 min, 4°C), the supernatant was recovered and EthR or EthR-G106W was separated from the whole-cell lysate by Ni-NTA agarose chromatography (Qiagen). After three washing steps with lysis buffer, His_6-tagged proteins were eluted from the resin with 250 mM imidazole in lysis buffer, dialyzed overnight against EthR Buffer (10 mM Tris/HCl, 300 mM NaCl, pH 7.5, 1 mM DTT, 0.1 mM EDTA). Protein purity was controlled by Coomassie blue staining after SDS–PAGE on a 12% polyacrylamide gel. Protein concentration was evaluated using the Bio-Rad protein assay kit. Purified proteins EthR and EthR-G106W were stored in EthR Buffer at 4°C.

Synthesis of EthR ligands

BDM14801, BDM31343 and BDM31381 were synthesized according to published procedures (14,16,17). BDM33066 [(S)-2-Amino-3-methyl-1-[4-(3-thiophen-2-yl-1,2,4-oxadiazol-5-yl)-piperidin-1-yl]-butan-1-one hydrochloride] was synthesized as follow: *N*-Boc-L-Valine (1.2 eq.), EDCI (1.2 eq.), HOBt (0.5 eq.) and triethylamine (4 eq.) were mixed in DCM (2 ml) for 5 min. Then 4-(3-Thiophen-2-yl-[1,2,4]oxadiazol-5-yl)-piperidine hydrochloride (150 mg, 0.5 mmol, 1 eq.) in 3 ml of DCM was added. The reaction mixture was stirred overnight at room temperature then evaporated under reduced pressure. The residue was purified by thick layer chromatography (DCM/MeOH 98/2) (Yield = 61%). Boc intermediate was deprotected using hydrogen chloride 4 N solution in dioxane (5 eq.). The residue was purified by thick layer chromatography (DCM/MeOH 9/1) to give BDM33066. Yield 66%; ^{1}H NMR (MeOD) δ 7.78 (dd, $J = 3.6$ Hz $J = 1.2$Hz, 1H), 7.68 (dd, $J = 5.1$Hz $J = 1.2$Hz, 1H), 7.20 (dd, $J = 5.1$Hz $J = 3.6$ Hz, 1H), 4.40–4.59 (m, 1H), 4.23–4.30 (m, 1H), 3.99–4.09 (m, 1H), 3.41–3.46 (m, 2H), 3.00–3.18 (m, 1H), 2.13–2.29 (m, 3H), 1.81–2.01 (m, 2H), 1.10 (d, $J = 7.2$Hz, 3H), 1.02 (d, $J = 6.9$ Hz, 3H). $t_{R\,LCMS}$ 3.9 min. Purity 99% MS $[M + H]^+$ m/z 335. NMR spectra were recorded on a Bruker DRX-300 spectrometer. Chemical shifts are in parts per million (ppm). Mass spectra were recorded with a LC-MSMS triple-quadrupole system (Varian 1200 ws). LCMS analysis was performed on a C18 TSK-GEL Super ODS 2 μm particle size column, 50 × 4.6 mm using a gradient starting from 100% H_2O/0.1% formic acid and reaching 20% H_2O/80% CH_3CN/0.08% formic acid within 10 min at a flow rate of 1 ml/min.

Crystal structure of $EthR_{G106W}$ and ligand complexes

Prior to crystallization, the protein was buffer exchanged against 10 mM Tris–HCl (pH 7.5), 200 mM NaCl and concentrated to 9 mg/ml. We obtained crystals of $EthR_{G106W}$, and cocrystals of EthR with ligands BDM33066 and BDM31343 by the vapor diffusion method. $EthR_{G106W}$ and EthR-BDM33066 were crystallized using 0.17 M ammonium sulfate, 0.085 M sodium cacodylate (pH 6.5), 15% glycerol and 25–35% polyethylene glycol 8000 as the crystallization solution. Co-crystals of EthR-BDM31343 were produced using 1.4–1.65 M ammonium sulfate (using 0.05 M increment), 15% glycerol and 0.1 M MES pH 6.7. The EthR ligand complexes were prepared by mixing 1 μl of ligand (33 mM in 100% DMSO) and 9 μl of the purified protein (9 mg/ml). Crystal structures of EthR in complex with BDM14801 (PDB#3O8G) and BDM31381 (PDB#3G1M) were reported previously (14,16).

All crystal obtained belong to space group $P4_12_12$, and thus displays a packing similar to the WT and other previously solved EthR structures. Data collection statistics for all structures are reported in Table 1. Diffraction data were processed with X-ray Detector Software (http://xds.mpimf-heidelberg.mpg.de/) (18). Phasing for the G106W mutant was accomplished by positioning the WT EthR structure using a rigid body minimization procedure, whereas phasing of liganded EthR structures were achieved by molecular replacement method using MolRep program (19). Structure refinements were done with program REFMAC5 (20) from the CCP4 suite (21). The G106W mutation was clearly visible in the electron density map. The Trp residue at position 106 was introduced and fitted into the electron density map using Coot (22) as well as the corrections of the conformation of adjacent residues. The final R_{factor} at 1.86 Å resolution is 17.7% (R_{free} of 22.9%) with a good geometry for the structure. The coordinates of the $EthR_{G106W}$ mutant and co-crystals of EthR with BDM33066 and BDM31343 have been deposited with the PDB data bank under the accession codes 3TP3, 3Q0W and 3TP0, respectively. Data collection and refinement statistics for all structures are reported in Table 1. Figures were prepared with PyMOL (http://www.pymol.org/).

Structural alignment of the different EthR structures was performed with Pymol and pairwise structure comparisons with DaliLite program (23). Supplementary Table S1 shows the RMS values obtained by pairwise structure superposition of the dimerization domain (from Lys68 to the C-terminus) of the six-liganded EthR structures.

Surface plasmon resonance binding assay

Real-time analysis of molecular interactions between EthR and the *ethA* promoter region was conducted on a Biacore™ 2000 apparatus (GE Healthcare). The *ethA–ethR* intergenic region was obtained by PCR using H37Rv chromosomal DNA as template and the following oligonucleotides: O-270: 5′-CGGTCATGGATCCACGC TATCAAC-3′ and O-271: 5′-biotin-CTGACTGGCCGC

Table 1. Data collection and refinement statistics

	$EthR_{G106W}$	EthR-BDM33066	EthR-BDM31343
Data collection			
X-ray source	rotating anode	ESRF ID23	SLS PXIII
Space group	$P4_12_12$	$P4_12_12$	$P4_12_12$
Cell dimensions			
A, *b*, *c* (Å)	119.7, 119.7, 33.7	119.8, 119.8, 33.6	119.1, 119.1, 33.6
α, β, γ (°)	90	90	90
Resolution (Å)	1.86 (1.86–1.91)[a]	1.6 (1.6–1.7)	1.89 (1.89–1.94)
$I/\sigma I$	22.1 (4.9)	17.7 (4.1)	17.8 (4.3)
Completeness (%)	97.75 (91.8)	99.8 (100)	100 (100)
Refinement			
Resolution (Å)	1.86	1.6	1.9
No. reflections	19 529	31 208	18 656
R_{work}/R_{free}	17.7/22.9	19.2/23.3	19.2/25.6
No. atoms			
Protein	1531	1502	1470
Ligand/ion	–	23	21
Water	216	160	81
B-factors			
Protein	18.6	22.1	29.7
Ligand/ion	–	25	27.9
Water	32	33.7	41.1
RMSDs			
Bond lengths (Å)	0.013	0.028	0.022
Bond angles (°)	1.29	2.5	1.9

[a]Number in parentheses is the statistic for the highest resolution shell.

GGAGGTGGT-3′. The amplified biotinylated DNA was purified on a Qiaquick column (Qiagen) and sequenced for verification. Immobilization of the DNA was performed on a streptavidin-coupled CM5 Sensor Chip using the standard protocol provided with the Amine Coupling Kit (Biacore™). Briefly, streptavidin was injected at 500 ng/ml in 10 mM sodium acetate (pH 3.5) for 12 min at a flow rate of 10 µ/min. The biotinylated DNA (~69 kDa) was injected through each flow cell at 200 ng/ml to reach a 205 resonance unit (RU) stable fixation to streptavidin. We controlled the integrity and quantity of fixed DNA with a 120-s injection of 1.6 mM calf histone H1 (Sigma) at 10 µ/min. Binding experiments of EthR and EthR-G106W to DNA were conducted in EthR-Buffer at a flow rate of 20 µ/min at 25°C. The protein was injected at 0.3 µM (concentration of the monomer) in the running buffer until equilibrium was reached. The Sensor Chip was regenerated by a 60-s injection of 0.03% SDS. Final curves presented in this document are representative of experiments repeated a minimum of four times and were obtained by substraction of the signal corresponding to a control flow cell functionalized with a double stranded irrelevant DNA fragment (internal fragment of the *E. coli bla* gene).

Thermal shift assay

The fluorescent dye SYPRO Orange (Invitrogen) was used to monitor protein unfolding. This dye is environmentally sensitive and leads to an increase in fluorescence following exposure of hydrophobic regions during protein unfolding. The thermal shift assay was conducted in a Lightcycler 480 (Roche). The system contained a heating/cooling device for temperature control and a charge-coupled device (CCD) detector for real-time imaging of the fluorescence changes in the wells of the microplate. The final sample concentrations were 10 µM EthR, 2.5× SYPRO Orange, 1% DMSO and 20 µM ligand in EthR buffer (10 mM Tris/HCl, 300 mM NaCl, pH 7.5, 1 mM DTT, 0.1 mM EDTA). Samples were heated from 37°C to 85°C with a heating rate of 0.04°C/s. Protein unfolding was monitored by recording changes in the fluorescence of SYPRO Orange. Fluorescence intensity was measured at Ex/Em: 465/510 nm. The inflection point of the curves was determined by plotting the first derivative dFI/d*T*, and the melting temperatures (T_m) were assessed from the maxima.

NMR spectroscopy

Proton spectra were recorded on a 27-mg/ml EthR sample in 300 mM NaCl, 10 mM Tris-d7 pH 7 aqueous buffer, at 30°C. Spectra were recorded with 128 scans on a 600-MHz AvanceI Bruker spectrometer (Karlsruhe, Germany) equipped with a cryogenic triple resonance probe head, and used excitation sculping for water suppression (24). Ligand BDM31381 was dissolved in DMSO-d6 and added to the EthR sample at a 1:1 ratio and at a final concentration of 1% DMSO-d6. An equivalent experiment using 1% DMSO-d6 without ligand was done to verify that DMSO at this concentration does not alter the spectrum of the apo-protein. The concentration of $EthR_{G106W}$ was 15 mg/ml, and spectra were recorded with 512 scans.

Isothermal titration calorimetry

ITC experiments were conducted in a VP-ITC Unit (MicroCal, Northampton, MA, USA), with 12.5 µM EthR (wild-type or G106W variant) in the cell

compartment and 0.3 mM of BDM14801 in the titrating syringe. ITC curves presented in this document are representative of experiments repeated four times with EthR WT and two times with the G106W variant. Both protein and ligand were prepared in EthR buffer containing 1% DMSO and without DTT. The protein was titrated at 25°C with 40×5 µl injections of the ligand. The duration of each injection was 10 s with 240 s spacing. The stirring speed during the titration was 300 rpm. Data were analyzed using Microcal Origin software by fitting the curves to a single-site binding model.

RESULTS

Determination of the minimal ligand binding site of EthR

Crystal structures of six holo-forms of EthR were chosen for tridimensional superimposition (Figure 1). The two first structures are holo-forms of EthR involving ligands fortuitously co-crystallized with the repressor. The first structure shows the 24-carbon long ligand (hexadecyl Octanoate, PDB access#1U9N) invading each of the hydrophobic pockets existing in the two monomers forming EthR (Figure 1a) (3). The 3D structure of the second crystal (PDB access#1T56) is nearly identical to the structure 1U9N (0.67 Å RMSD) but instead of one long linear hydrophobic ligand, this crystal exhibits two dioxanes embedded in each monomer of EthR (Figure 1b) (12). Co-crystals of EthR with four synthetic compounds are also depicted in Figure 1c–f. BDM14801 (PDB#3O8G), BDM31381 (PDB#3G1M), BDM31343 (PDB#3TP0) and BDM33066 (PDB#3Q0W) are compounds that bear two hydrophobic ends connected by a 4–6-Å linker (14). These compounds where initially designed to 'mimic' the mode of binding of the two cyclic compounds present in the ligand binding pocket of 1T56 and to offer hydrogen bonding capabilities set to interact with Asn176 and Asn179 of EthR. In all four cases, the co-crystals revealed that occupation of the binding pocket by these compounds induces structural reorganization of the HTH regions equivalent to the one observed in crystal structures 1T56 and 1U9N. More precisely, in the six cases analyzed here, distance between the P59 (C_α) of each HTH motifs [corresponding to P39 in TetR (25) and to G37 in QacR (26)] are comprised between 42 and 47 Å. These HTH spacings are much larger than the 34- to 37-Å distance observed in co-crystallized repressor-operator complexes (26–30).

In contrast to this consistent structural effect, the localizations of these various ligands in the hydrophobic pocket of EthR as well as their interactions with various amino acids of the protein are rather heterogeneous. The hexadecyl-octanoate embedded in structure 1U9N is ~27 Å long and thus potentially contacts >30 amino acids delimiting the ligand pocket of EthR, including some deeply located in the pocket close to the HTH domain. On the other hand, the two small cyclic molecules described in 1T56 are located respectively in the upper and mid part of the pocket and thus, contact a much more limited number of amino acids. As depicted in two previous reports, BDM31381 and BDM14801 occupied the same region than the one in contact with the two dioxane of 1T56 (14,16). The co-crystal EthR-BDM31343 presented here led to the same observation, confirming the implication of this portion of the pocket in the structural induction of the repressor. Moreover, these three ligands are hydrogen-bonded to the side chain of N179 through their common amide function. Recently, we performed an extensive structure-activity relationship study of BDM31343, which included the replacement of its cyanoacetyl group (15). Some of the ligands identified during this process were cocrystallized with EthR. Surprisingly, BDM33066 revealed to be located higher in the binding pocket of EthR and in the opposite orientation compared to its progenitor BDM31343 (Figure 1e). As such, the thiophene moiety of BDM33066 occupied the region corresponding to the uppermost dioxane described in structure 1T56. Nevertheless, these limited ligand–protein contacts were sufficient to promote a structural reorganization of the HTH motifs globally equivalent to the one observed with the other compounds.

Superimposition of these six structures of EthR co-crystallized with fortuitous or synthetic ligands revealed very weak tridimensional variations (pairwise RMSD in the range of 0.3–0.7 Å; see Supplementary Table S1), and thus allowed to delimit a narrow tridimensional space shared by all compounds. As illustrated in Figure 1g, this space corresponds to the C_{18}–C_{20} portion of hexadecyl-octanoate, to the upper dioxane present in structure 1T56, to the piperidine group of either BDM31381, BDM14801 or BDM31343, and to the thiophene portion of BDM33066. These observations invited us to hypothesize that contacts between ligands and EthR within this very limited region of the pocket could be sufficient to initiate a spatial reorganization of the two HTH motifs of the repressor leading to a conformation incompatible with DNA binding.

The superimposition of the ligands not only allowed to point amino acids of the pocket potentially involved in the structural switch of EthR but also revealed some strong spatial constrains imposed to all ligands in this region. As illustrated in Figure 2a, the spatial portion common to all ligands share the same geometry plane.

We then hypothesized that both steric and spatial hindrance imposed by the ligands to this portion of the binding pocket could be mimicked by the side chain of an amino acid artificially introduced in this region of the protein, advantageously by an amino acid residue bearing a planar hydrophobic side chain such as phenylalanine, tyrosine or tryptophane.

Systematic substitution of amino acids located in this region of the ligand binding pocket by hydrophobic residues was simulated using the mutagenesis tool of Pymol (Mutagenesis Wizard, Schrodinger, LLC). Replacement of amino acids A83, L87, L90, M102, G106, T149, V152 and L175 by Phe, Tyr or Trp were evaluated (data not shown). Replacement of G106 by Trp (Figure 2b) was the most promising change that could advantageously mimic the encumbrance of the common portion of all ligands (the piperidine group of

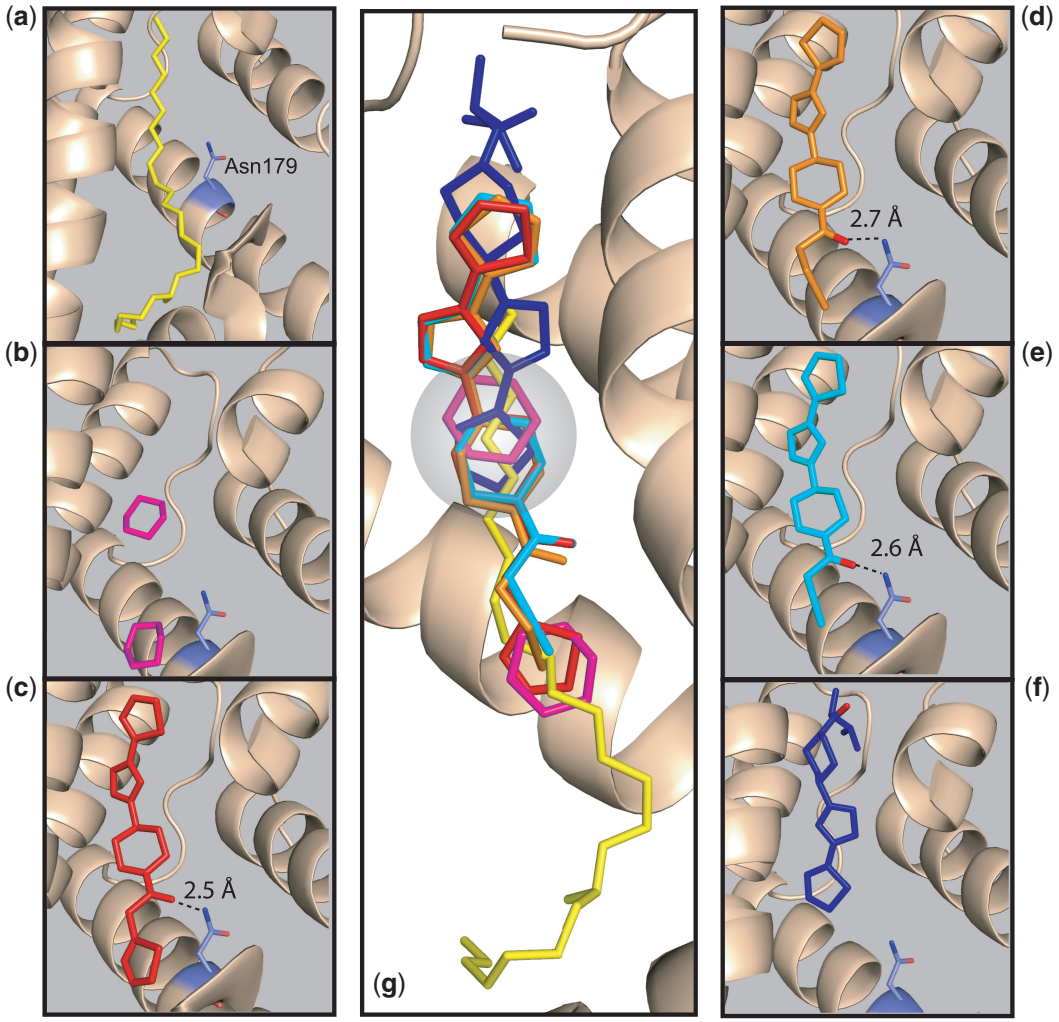

Figure 1. Determination of the 'minimal ligand binding site' of EthR. Crystal structure of the ligand binding site of six holoforms of EthR: (**a**) EthR-hexadecyl-octanoate (PDB#1U9N), (**b**) EthR-Dioxane (PDB#1T56), (**c**) EthR-BDM31381 (PDB#3G1M), (**d**) EthR-BDM14801 (PDB#3O8G), (**e**) EthR-BDM31343 (3TP0) and (**f**) EthR-BDM33066 (PDB#3Q0W). Close-views of the occupancy of each ligand in the binding pocket of EthR. The protein is displayed in ribbon and the side chain of Asn179 is represented by sticks colored according the following atom color schemes: carbon in blue, oxygen in red and nitrogen in dark blue. When observed, hydrogen bonds with this latter side chain are depicted by dashed lines with the interacting distance indicated. (**g**) Superimposition of the six crystal structures. The cyclic moieties of BDM14801 (orange), BDM31381 (red), BDM33066 (dark blue), BDM31343 (light blue), the C_{18}–C_{20} portion of hexadecyl-octanoate (yellow) and the upper dioxane (pink) share a narrow space delimited with the gray translucent disk.

either BDM31381, BDM14801 and BDM31343, the thiophenyl group of BDM33066 or the upper dioxane present in 1T56).

EthR mutagenesis and crystal structure

Mutation G106W was introduced in His-tagged EthR by side direct mutagenesis, the protein was produced in *E. coli* and purified on Nickel-affinity column. The crystal structure of $EthR_{G106W}$ was determined at a resolution of 1.86 Å starting from the coordinates of the wild-type protein, allowing to evaluate the structural impact of the G106W mutation. The obtained crystals belong to space group $P4_12_12$ with unit cell parameters $a = b = 119.7$ Å and $c = 33.7$ Å which corresponds to the space group obtained in our previous studies of liganded EthR (3), demonstrating that mutation G106W does not destabilize or deeply modify the overall structure of the repressor.

Detailed analysis of this structure revealed that the values of backbone dihedral angles phi/psi do not change upon mutation G106W, remaining around −70°/−50°. Thus, the indole group of W106 (Figure 3a) occupies the volume otherwise filled by the common portion of ligands, for instance the thiophene moiety of BDM33066 (Figure 3b).

Interestingly, the electron density map revealed that $EthR_{G106W}$ is a ligand-free protein. Compared to the pocket containing hexadecyl-octanoate observed in structure 1U9N, the absence of ligand in $EthR_{G106W}$ permits the reorganization of some amino acids (Figure 3c). The benzyl side chain of F141 is now tilted inside the empty pocket, which forces the indole group of W145 to rotate 180° upwards, thus filling the free space located

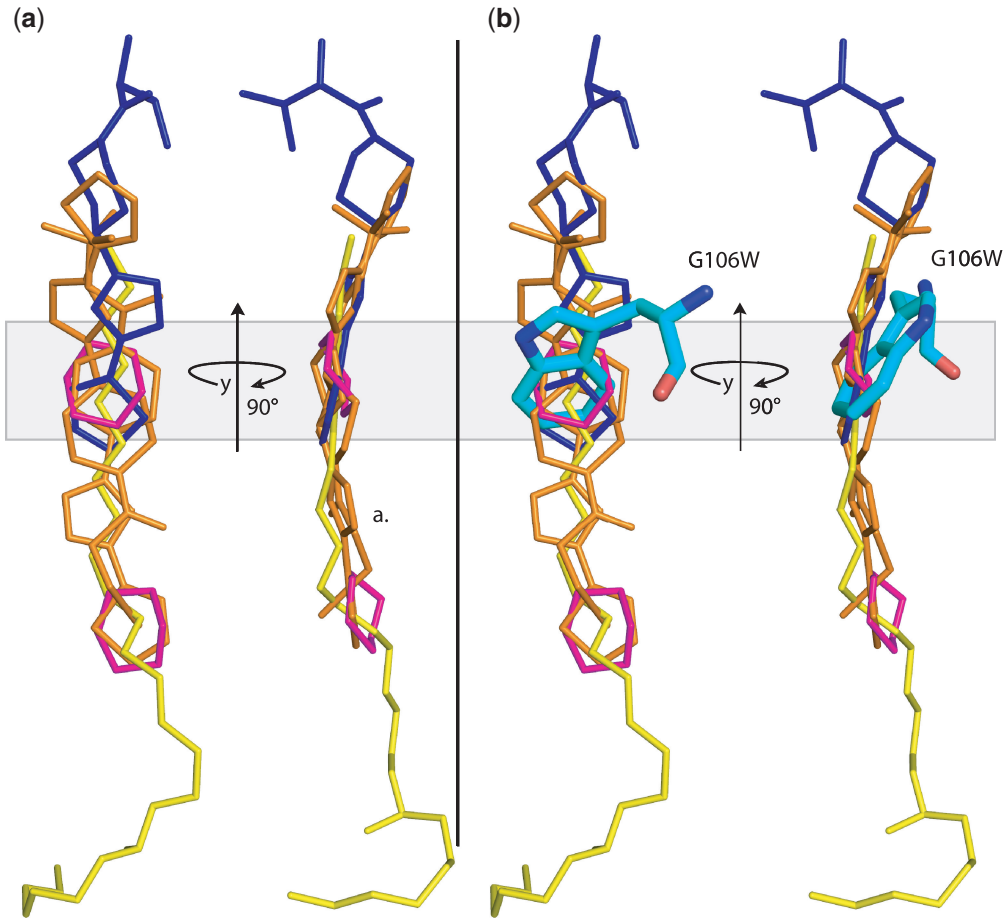

Figure 2. *In silico* mutagenesis model of G106W. (**a**) Front and 90° lateral views of the superimposition of the ligands in their respective position in the ligand binding pocket of EthR. The gray rectangle highlights the zone common to all ligands. (**b**) Front and 90° lateral views of the *in silico* substitution of glycine 106 for tryptophan.

in-between L87 and K144, also resulting in a slide push of Y148 (Figure 3c). Changes are also observed in the bottom part of the pocket. The side chains of F184 and Q125 now invade the empty ligand binding pocket and R128 freely spreads out its side chain perpendicularly to the tunnel (Figure 3c). The most important observation refers to the conformation of the DNA binding motifs of this variant of EthR. Even though this mutated protein does not contain any ligand in its binding pocket, X-ray data revealed that the distance separating the P59 (C_α) of each HTH motifs is 42.3 Å (Figure 3d).

Binding of $EthR_{G106W}$ to DNA

With its DNA recognition helices α3 and α3′ separated by 41.5 Å, the G106W variant of EthR was predicted to be unable to bind its DNA operator, as this distance amply exceeds the helical periodicity of the B-DNA double helix (34 Å per turn of the helix). However, it could be possible that the conformation revealed by the crystal structure reflects a peculiar conformational state of $EthR_{G106W}$ that is not necessarily representative of the conformation and dynamics of the protein in solution (31). Thus, the capacity of the variant repressor $EthR_{G106W}$ to interact with its DNA operator in solution was investigated by surface plasmon resonance (SPR) and compared to that of EthR. As described previously (9), EthR bound specifically and cooperatively to its 55 bp operator located in the intergenic region separating *ethA* and *ethR*. On the contrary, injection of $EthR_{G106W}$ onto the same sensorchip revealed a total absence of interaction with the DNA operator (Figure 4). This data experimentally confirms that mutation G106W abolishes the capacity of binding of $EthR_{G106W}$ to its DNA operator in solution, in agreement with the HTH architecture of the variant repressor revealed by X-ray crystallography (Figure 3d).

Comparative folding behavior properties of $EthR_{G106W}$ and EthR

Crystallography studies revealed that variant protein $EthR_{G106W}$ is in a conformation equivalent to the one observed in ligand–EthR co-crystals and that both situations translate in incompatibility with DNA binding as measured by SPR. Hence, we attempted to compare the impact on folding stability of the G106W mutation with the one resulting from the binding of specific ligands to the repressor. Monitoring of the thermal unfolding was performed using a fluorescence-based thermal shift

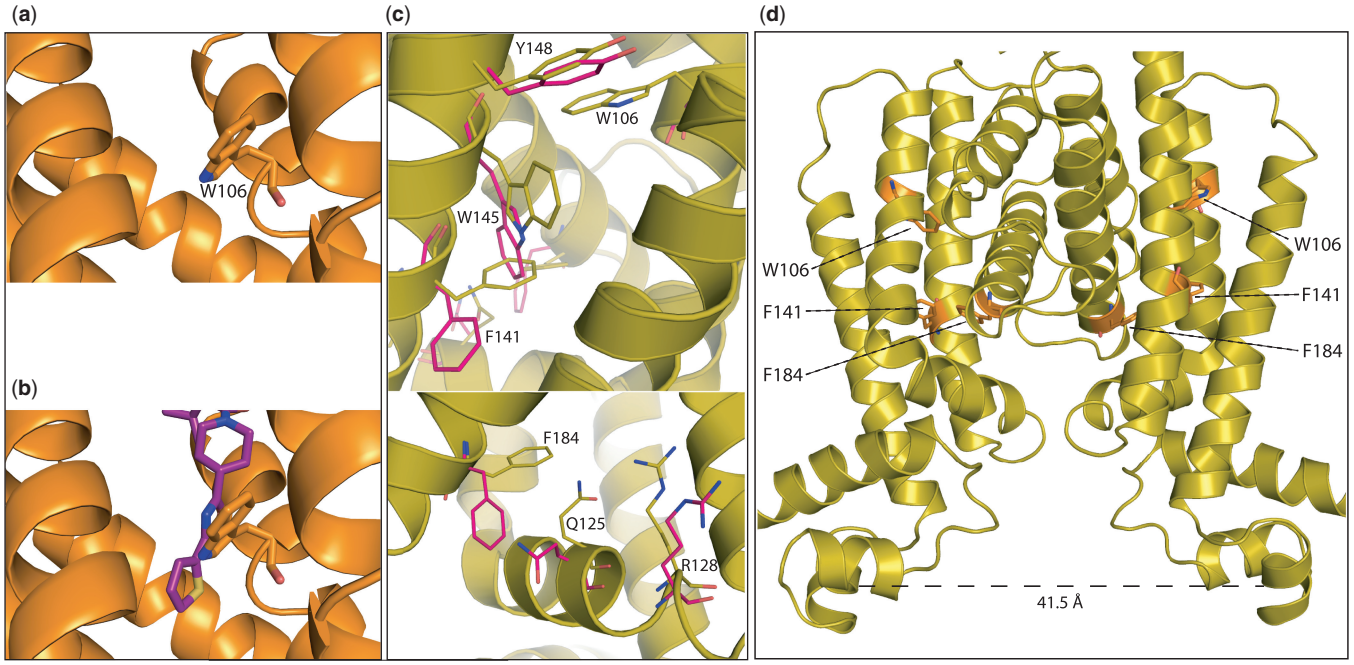

Figure 3. Crystallographic structure of $EthR_{G106W}$. (**a**) Close view of the indole group of tryptophan 106 as observed in the crystal structure of the variant $EthR_{G106W}$ (PDB#3TP3). (**b**) Close view of the same region superimposed with the crystal structure of EthR-BDM 33066 (ligand BDM 33066 is shown in purple). (**c**) Superimposition of $EthR_{G106W}$ (Gold) and EthR-hexadecyl-octanoate (Pink). Only selected amino acid side chains are shown. Reorganization of amino acid side chains in the north part (upper panel) and in the south part (lower panel) of the ligand binding pocket. (**d**) Measurements of the distance separating the two helix-turn-helix DNA-binding motifs (α carbon of P59's) in the variant $EthR_{G106W}$.

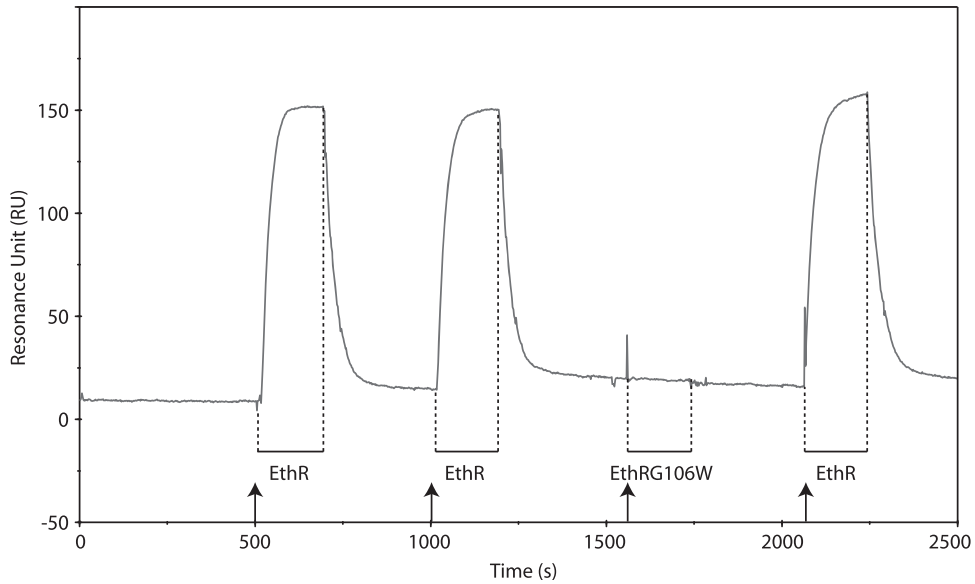

Figure 4. Binding of EthR and $EthR_{G106W}$ to the DNA operator of *ethA* measured by surface plasmon resonance. Sensorgram showing two successive injections of 0.3 µM EthR (at 500 and 1000 s) on a sensor chip functionalized with 250 arbitrary RU of the biotinylated intergenic *ethA-R* DNA region (9), followed by the injection of 0.3 µM $EthR_{G106W}$ (at 1600 s). A third injection of 0.3 µM EthR was done (at 2100 s) to control the binding capacity of the chip after the previous injection of $EthR_{G106W}$. Arrows indicate time of protein injection.

assay (TSA) (32,33). The method takes advantage of the differential behavior of hydrophobic fluorophores upon exposure to folded or to unfolded protein. The fluorescence of probes such as SYPRO Orange is quenched in aqueous solution but is restored when it contacts hydrophobic regions of protein exposed upon unfolding. Fluorescence emission can be studied as a function of temperature, which provides a melting curve revealing the thermal stability of a protein or complexes. The thermal unfolding curves of EthR and $EthR_{G106W}$ were

determined using a Q-RT-PCR thermo cycler (Light Cycler Roche 480). As shown in Figure 5a, the unfolding of EthR and $EthR_{G106W}$ followed a two-state transition as the fluorescence intensity (FI) increased during the progressive unfolding of the protein, reached the plateau and then decreased due to aggregation of denatured

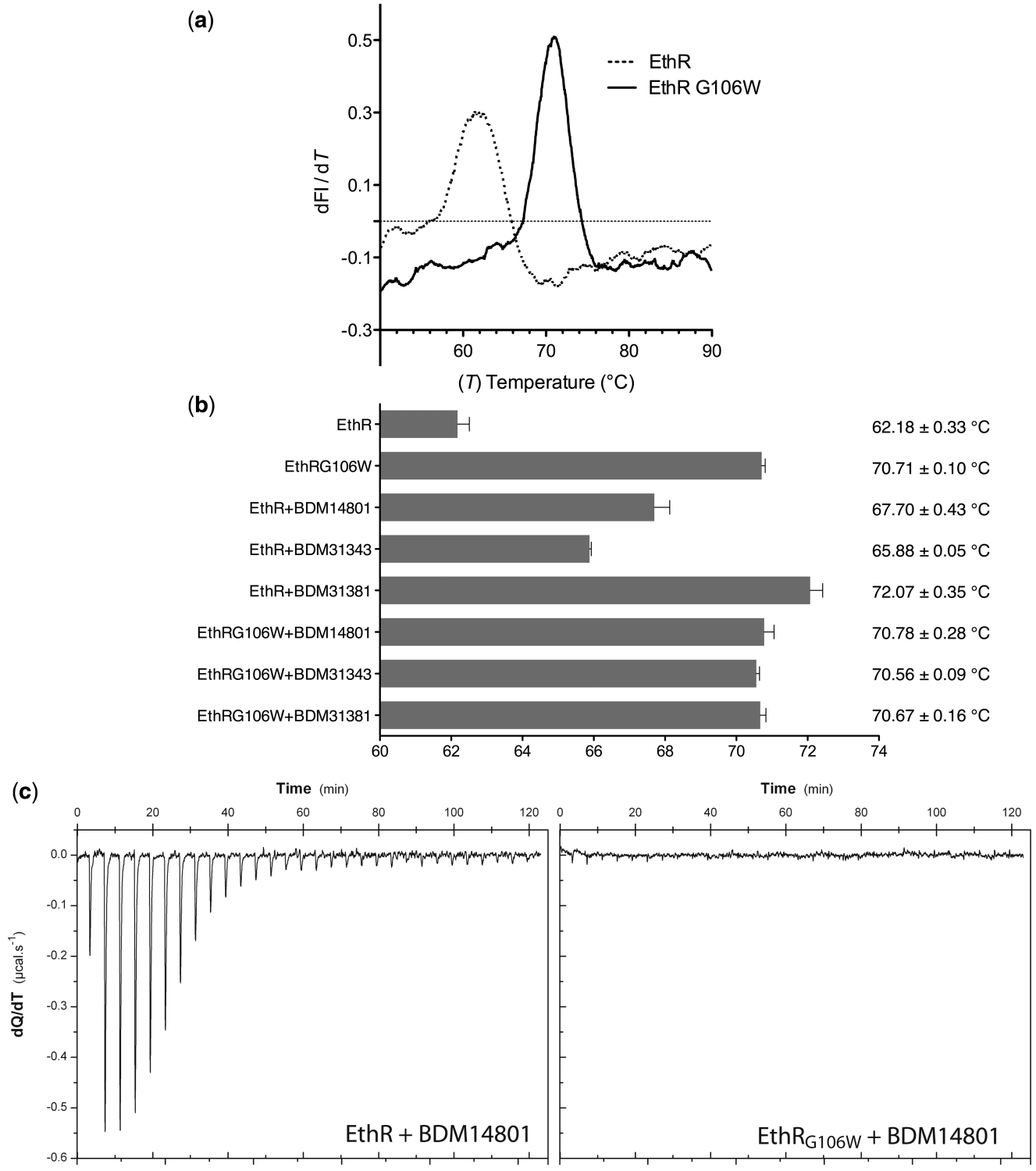

Figure 5. Binding of ligands to EthR and $EthR_{G106W}$. (**a**) Thermal stability of EthR (dashed curve) and $EthR_{G106W}$ (plain curve). Curves correspond to the first derivative of the fluorescence of Sypro Orange recorded during samples denaturation (30 values per °C). Melting temperature (T_m) for each sample corresponds to the maxima of the curve. (**b**) T_m of EthR and $EthR_{G106W}$ in the presence of indicated ligands. (**c**) Isothermal Titration Calorimetry study of the binding of BDM14801 to EthR (left) and $EthR_{G106W}$ (right). The graph shows raw data of a typical experiment, expressed in µcal/s versus time units.

protein–dye complex (32). Respective melting temperatures (T_m) were deduced by extracting the maximum of the first order derivative of the melting curves fluorescence data (dFI/dT). Under equivalent experimental conditions, the average T_m of EthR and of $EthR_{G106W}$ were respectively 62.2°C ± 0.3 and 70.7°C ± 0.1, revealing a much higher thermal stability of the variant protein compared to the wild-type (Figure 5a).

We then compared the stabilization effect brought by the G106W mutation with the one obtained when EthR was mixed with various known synthetic ligands. Three synthetic ligands (BDM14801, BDM31343 and BDM31381) of EthR were selected based on their capacities to inhibit EthR–DNA interactions *in vitro* (14,16). The thermal stability curves corresponding to the three complexes EthR-BDM14801, EthR-BDM31343 and EthR-BDM31381 were recorded and compared to the ones obtained for EthR and $EthR_{G106W}$. Figure 5b shows that BDM31381 is the compound that induced the highest T_m when it binds to EthR (72.1°C ± 0.4), followed by BDM14801 with 67.7°C ± 0.5 and by BDM31343 with a T_m of 65.9°C ± 0.1. Interestingly, thermostability gain associated to mutation G106W appears more important than the one observed when EthR was mixed with ligands BDM31343 and BDM14801, and slightly less important than the one observed for the complex EthR-BDM31381. Altogether, these data correlated well with our previous SPR results showing that BDM31381 was more efficient than BDM14801, itself more active than BDM31343 in impairing the capacity of EthR to bind its DNA operator (14). In conclusion, the thermal stabilization of EthR brought by mutation G106W is equivalent to the one brought by highly efficient ligands of the repressor.

To test whether high affinity EthR ligands could force a relocalization of the indole side chain of W106 to invade the pocket, we measured the capacity of the three ligands to improve the thermal stability of $EthR_{G106W}$. None of them was able to modify the midpoint transition temperatures of the mutated protein (Figure 5b). Interestingly, even BDM31381, with its ability to stabilize the WT protein at a temperature superior than the melting temperature of $EthR_{G106W}$, was unable to modify the melting temperature of the variant protein.

As it cannot be excluded that interaction of ligands with $EthR_{G106W}$ is undetectable by TSA due to the high thermostability of this variant protein, we used isothermal titration calorimetry. We first measured whether the formation of the EthR-BDM14801 complex is exothermic or endothermic. Figure 5c (left panel) shows a typical titration at 25°C of EthR (12.5 μM) by serial injections of BDM14801 (0.3 mM). This experiment revealed that heat was released when EthR associated with this ligand. A similar experiment was repeated to determine whether BDM14801 interact with the variant protein $EthR_{G106W}$. As shown in Figure 5c (right panel), no heat change could be detected when 0.3 mM BDM14801 was injected into the adiabatic cell containing 12.5 μM $EthR_{G106W}$. This result confirms that the variant protein $EthR_{G106W}$ has completely lost its capacity to interact with ligands that bind the wild-type protein with a high affinity.

Probing the protein dynamics with NMR spectroscopy

Altogether the parallelism between the mechanism of inhibition by ligands and by the G106W mutation suggests that the increased rigidity of the structure in an 'open HTH form', which translates in the observed improved thermostability, may be the underlying mechanism leading to the loss of the DNA-binding function of EthR (34). To collect direct evidence for a possible mechanism of ligand-induced rigidification that would be paralleled by the G106W mutation, we performed NMR spectroscopy of the proteins in the absence and presence of ligands. Whereas heteronuclear NMR of the 50-kDa dimer is beyond reach at this moment, we focused on the well-resolved upfield shifted methyl resonances. Chemical shift prediction by ShiftX2 (35) based on the crystal structures identified a number of methyls with upfield shifted resonances, mainly belonging to residues that surround the hydrophobic ligand binding pocket (Supplementary Figure S1). Although the prediction itself might not be reliable enough to assign them individually, the set of methyl resonances detected at resonance frequencies <0.5 ppm is expected to correspond to those methyls. In the apo-EthR spectrum, they are hardly detectable as broad humps, but they do significantly sharpen in the presence of ligand BDM31381 (Figure 6, lower and middle traces). As the size of the dimeric complex and subsequent slow tumbling do not vary upon ligand binding, we can exclude these factors as sole source of line broadening. Slow movements of the apo-protein on the micro- to millisecond time scale equally can contribute to peak broadening in a process called 'exchange broadening' (36), whereas these latter movements appear quenched upon ligand binding. Most importantly, however, we observe similar sharp lines directly with the G106W variant, before adding any ligand (Figure 6, upper trace). This unambiguously indicates that the influence of the ligand on the motional regime at equilibrium (in the thermodynamic sense) is mimicked in a good manner by the sole G106W mutation. The average position of the side chains predicted with upfield shifted methyls does not vary between the ligand bound WT and G106W mutant proteins, as evidenced by our crystal structures, explaining why these resonances do not shift their position.

DISCUSSION

EthR is a transcriptional regulator of the TetR family. EthR regulates the production of EthA, a monooxygenase implicated in the bioactivation of the antimycobacterial prodrug ETH. Our previous works showed that synthetic compounds mimicking fortuitous ligands of EthR inhibit EthR, and consequently, increase ETH bioactivation through the overproduction of EthA. Inhibition of the DNA binding function of EthR by these ligands follows a mode of action typical in the TetR family of repressors. In these dimeric regulators, invasion of the binding pockets by specific ligands results in the structural modifications of the helix-turn-helix motifs of each monomer, which translates in the loss of DNA recognition and

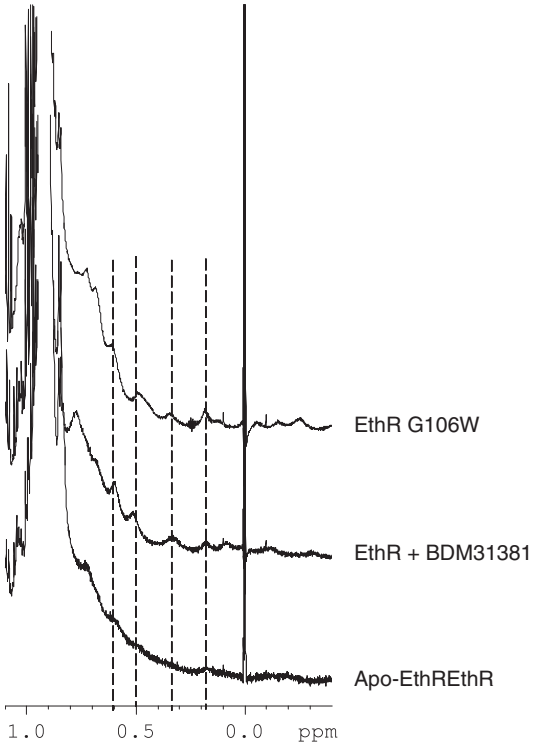

Figure 6. Upfield region of the 1D proton spectrum of apo-EthR (bottom), EthR + ligand BDM31381 (middle) and apo-$EthR_{G106W}$ (top). Signals in this region correspond to methyl protons whose resonance is shifted out of the crowded methyl region (1.5–0.8 ppm) by the ring current effect of nearby aromatics (Full NMR spectra are shown in Supplementary Figure S2). Prediction by ShiftX2 (35) shows plausible candidates (Supplementary Figure S1). Whereas these resonances are severely broadened in the apo-EthR spectrum, they sharpen significantly upon ligand addition or in the G106W mutant. Resonances with conserved frequencies have been indicated by dotted vertical lines. Differences between the most shifted resonances in the EthR-ligand and $EthR_{G106W}$ mutant could come from a differential magnetic influence of the ligand and the Trp side chain, and cannot necessarily be interpreted in terms of structural differences.

binding to the repressor. The allosteric effect of the ligand, meaning the structural mechanism by which binding of molecules in the ligand pocket lead to the structural organization of distant motifs, is still not fully understood.

In the case of EthR, highly diverse ligands provoke the structural modifications leading to a conformation incompatible with DNA binding. This was shown with molecules as different as the 24-carbon long hexadecyl octanoate, small cyclic molecules such as dioxane, or various structure-based designed synthetic inhibitors. Here, we aligned liganded-EthR structures in order to identify structural similarities that may explain how chemically diverse ligands exert a common inhibitory effect on EthR. Interestingly, the common portion of the binding pocket of EthR that is in contact with every ligand is very limited. In addition, intensive structure activity relationship studies done to improve our synthetic ligands demonstrated that important structural constrains are required to allow ligand compatibility in this region (14–16, M. Flipo *et al.*, submitted for publication). The goal of the actual study was to test whether this limited zone of the pocket could be the hot-spot leading to the allosteric response observed upon ligand binding, which impact the spatial architecture of the helix-turn-helix motifs of the repressor. Mutagenesis of glycine 106 to tryptophan was introduced in order to mimic the effect of ligands in this region of the pocket. This mutation entailed structural modifications and thermostabilization of the repressor equivalent to what was observed in the presence of ligands.

First, X-ray structural analysis revealed that the HTH DNA binding motifs of the mutated repressor are in a conformation incompatible with DNA binding. Indeed, $EthR_{G106W}$ shows a structural spacing of its HTH domains (42.3 Å) in the range observed in ligand–protein complexes (42 Å with BDM31343 to 47 Å with BDM14801) reinforcing the idea of mechanistic mimicry between mutation G106W and ligands. Consistently, the mutated repressor showed a complete incapacity to bind to its DNA operator. Nevertheless, in their apo-form that is by nature competent for DNA binding, the majority of the regulators of the TetR family crystallizes in a conformation clearly not compatible with DNA binding (37). These observations led some authors to postulate that crystal structures of apo-repressors of the TetR family reflect only a snap shot of the conformational repertoire of the proteins in solution and that the role of ligands could be to stabilize one conformation of the repertoire in which the recognition helices are too far apart to simultaneously bind to adjacent major groove of DNA (31,34,38).

If true, this stabilization should naturally translate in some rigidification of the protein upon binding of ligand. Interestingly, the $EthR_{G106W}$ crystal reveals the first apo form of EthR. Our inability to succeed in the crystallization of apo-form of the wild-type EthR suggest that the major effect of the mutation, mimicking ligands, was to improve the global stability of the protein. Preliminary NMR experiments are in support of this hypothesis, showing that a number of methyls of the protein have indeed their NMR signal affected by exchange broadening, reflecting typical dynamic processes on the micro- to millisecond time scale, but both the presence of ligand and the G106W mutation quench this dynamics (Figure 6; Supplementary Figures S1 and S2). From a thermodynamic point of view, fast internal dynamics of the ligand binding pocket of EthR have the potential to report on the number of states that the protein explores, hence, acting as an indirect measure of the residual entropy of the folded state. This observation could somehow remind the transcription factor ETS, for which flexibility was shown to be directly correlated to its capacity of binding to its DNA target (36).

Alternatively, the observed distance of >42 Å that separate the HTH motifs in either $EthR_{G106W}$ or in EthR–ligand complexes may by itself explain the inability of the repressor to bound to its DNA operator, and the drastic diminution of the internal flexibility observed in both cases could induce a locking mechanism to restrict further conformational change, as proposed recently by Le *et al.* (38) for SimR.

Intensive mutagenesis studies on TetR have led to the identification of many variants that are no longer able to

bind to DNA, whereas there still show good affinity for tetracycline (39,40). Conversely, other variants that bind DNA more strongly in the presence of tetracycline have been described (41–44). Here, we have identified a variant of EthR harboring the yet undescribed property to mimic the allosteric effect of known ligands, resulting in the complete inhibition of its DNA binding capacity. This mutation not only mimics the activity of small molecule ligands either at the functional level (inhibition of DNA binding propensity), but also at the structural level (equivalent structural conformations), or at the dynamic level (rigidification of the structure).

The design and improvement of high-affinity inhibitors in the context of drug discovery is a complex matter as the increase of enthalpy through increased bond strength is countervailed by the entropy reduction due to the global increase of order of the system. In allosteric systems, it is then essential to localize precisely the region of a protein implicated in ligand-induced signal in order to facilitate the design of structure-based inhibitors and maximize their entropic and enthalpic contributions. The present work used the large chemical and structural diversity of known EthR's ligands to identify one region of the protein implicated in the allosteric response of its DNA binding domain. Here, we have demonstrated that the inhibitory effect of highly diverse specific ligands of EthR can be mimicked by the mutation G106W. This now explains how two small cyclic molecules such as dioxane (12) induced the same conformational state as the one induced with hexadecyl-octanoate (3,13). Conversely, our results suggest that exploitation of deeper portions of the ligand pocket to increase their affinity/specificity would be successful as long as these molecules interact with the upper region of the pocket surrounding glycine 106.

ACCESSION NUMBERS

PDB: 3TP3, 3Q0W, 3TP0.

SUPPLEMENTARY DATA

Supplementary Data are available at NAR Online: Supplementary Table 1 and Supplementary Figures 1 and 2.

ACKNOWLEDGEMENTS

We are indebted to the ESRF (Group BAG MX-485). Diffraction data for BDM31343 and EthR-BDM33066 were collected at the Swiss Light Source (Paul Scherrer Institute, Villigen, Switzerland) and at the ESRF (Group BAG MX-485), respectively. We are grateful to the machine and beamline scientists whose outstanding efforts have made these experiments possible.

FUNDING

This work was supported by Institut Pasteur de Lille and the Région Nord-Pas de Calais (doctoral fellowship for X.C.); the Ministry of Education and Research (MENR) (doctoral fellowship for B.D.); Inserm; Univ. Lille Nord de France; CNRS; EU - Région Nord-Pas de Calais-FEDER (N°09220019 and N°09220020 PRESAGE 31510); and the Pôle de Recherche Interdisciplinaire pour le Médicament (PRIM). Funding for open access charge: INSERM.

Conflict of interest statement. None declared.

REFERENCES

1. Cox,H.S., Ford,N. and Reeder,J.C. (2009) Are we really that good at treating tuberculosis? *Lancet Infect. Dis.*, **9**, 138–139.
2. Mitnick,C.D., McGee,B. and Peloquin,C.A. (2009) Tuberculosis pharmacotherapy: strategies to optimize patient care. *Expert Opin. Pharmacother.*, **10**, 381–401.
3. Frénois,F., Engohang-Ndong,J., Locht,C., Baulard,A.R. and Villeret,V. (2004) Structure of EthR in a ligand bound conformation reveals therapeutic perspectives against tuberculosis. *Mol. Cell*, **16**, 301–307.
4. Zhang,Y., Heym,B., Allen,B., Young,D. and Cole,S. (1992) The catalase peroxidase gene and isoniazid resistance of *Mycobacterium tuberculosis*. *Nature*, **358**, 591–593.
5. Scorpio,A. and Zhang,Y. (1996) Mutations in pncA, a gene encoding pyrazinamidase/nicotinamidase, cause resistance to the antituberculous drug pyrazinamide in tubercle bacillus. *Nat. Med.*, **2**, 662–667.
6. Baulard,A.R., Betts,J.C., Engohang-Ndong,J., Quan,S., McAdam,R.A., Brennan,P.J., Locht,C. and Besra,G.S. (2000) Activation of the pro-drug ethionamide is regulated in mycobacteria. *J. Biol. Chem.*, **275**, 28326–28331.
7. DeBarber,A.E., Mdluli,K., Bosman,M., Bekker,L.G. and Barry,C.E. III (2000) Ethionamide activation and sensitivity in multidrug-resistant *Mycobacterium tuberculosis*. *Proc. Natl Acad. Sci. USA*, **97**, 9677–9682.
8. Qian,L. and Ortiz de Montellano,P.R. (2006) Oxidative activation of thiacetazone by the *Mycobacterium tuberculosis* flavin monooxygenase EtaA and human FMO1 and FMO3. *Chem. Res. Toxicol.*, **19**, 443–449.
9. Engohang-Ndong,J., Baillat,D., Aumercier,M., Bellefontaine,F., Besra,G.S., Locht,C. and Baulard,A.R. (2004) EthR, a repressor of the TetR/CamR family implicated in ethionamide resistance in mycobacteria, octamerizes cooperatively on its operator. *Mol. Microbiol.*, **51**, 175–188.
10. Ramos,J.L., Martinez-Bueno,M., Molina-Henares,A.J., Teran,W., Watanabe,K., Zhang,X., Gallegos,M.T., Brennan,R. and Tobes,R. (2005) The TetR family of transcriptional repressors. *Microbiol. Mol. Biol. Rev.*, **69**, 326–356.
11. Beckers,G., Strosser,J., Hildebrandt,U., Kalinowski,J., Farwick,M., Kramer,R. and Burkovski,A. (2005) Regulation of AmtR-controlled gene expression in *Corynebacterium glutamicum*: mechanism and characterization of the AmtR regulon. *Mol. Microbiol.*, **58**, 580–595.
12. Dover,L.G., Corsino,P.E., Daniels,I.R., Cocklin,S.L., Tatituri,V., Besra,G.S. and Futterer,K. (2004) Crystal structure of the TetR/CamR family repressor *Mycobacterium tuberculosis* EthR implicated in ethionamide resistance. *J. Mol. Biol.*, **340**, 1095–1105.
13. Frénois,F., Baulard,A.R. and Villeret,V. (2006) Insights into mechanisms of induction and ligands recognition in the transcriptional repressor EthR from *Mycobacterium tuberculosis*. *Tuberculosis*, **86**, 110–114.
14. Willand,N., Dirie,B., Carette,X., Bifani,P., Singhal,A., Desroses,M., Leroux,F., Willery,E., Mathys,V., Deprez-Poulain,R. *et al.* (2009) Synthetic EthR inhibitors boost antituberculous activity of ethionamide. *Nat. Med.*, **15**, 537–544.
15. Flipo,M., Desroses,M., Lecat-Guillet,N., Dirie,B., Carette,X., Leroux,F., Piveteau,C., Demirkaya,F., Lens,Z., Rucktooa,P. *et al.* (2011) Ethionamide boosters: synthesis, biological activity, and structure-activity relationships of a series of 1,2,4-oxadiazole EthR inhibitors. *J. Med. Chem.*, **54**, 2994–3010.

16. Willand,N., Desroses,M., Toto,P., Dirie,B., Lens,Z., Villeret,V., Rucktooa,P., Locht,C., Baulard,A. and Deprez,B. (2010) Exploring drug target flexibility using in situ click chemistry: application to a mycobacterial transcriptional regulator. *ACS Chem. Biol.*, **5**, 1007–1013.
17. Poulain,R.F., Tartar,A.L. and Déprez,B.P. (2001) Parallel synthesis of 1,2,4-oxadiazoles from carboxylic acids using an improved, uronium-based, activation. *Tetrahedron Lett.*, **42**, 1495–1498.
18. Kabsch,W. (1993) Automatic processing of rotation diffraction data from crystals of initially unknown symmetry and cell constants. *J. Appl. Cryst.*, **26**, 795–800.
19. Vagin,A. and Teplyakov,A. (1997) MOLREP: an automated program for molecular replacement. *J. Appl. Cryst.*, **30**, 1022–1025.
20. Winn,M.D., Isupov,M.N. and Murshudov,G.N. (2001) Use of TLS parameters to model anisotropic displacements in macromolecular refinement. *Acta Crystallogr. D. Biol. Crystallogr.*, **57**, 122–133.
21. Collaborative-Computational-Project-Number-4. (1994) The CCP4 suite: programs for protein crystallography. *Acta Crystallogr. D. Biol. Crystallogr.*, **50**, 760–763.
22. Emsley,P. and Cowtan,K. (2004) Coot: model-building tools for molecular graphics. *Acta Crystallogr. D. Biol. Crystallogr.*, **60**, 2126–2132.
23. Holm,L. and Park,J. (2000) DaliLite workbench for protein structure comparison. *Bioinformatics*, **16**, 566–567.
24. Stott,K., Stonehouse,J., Keeler,J., Hwang,T.S. and Shaka,A.J. (1995) Excitation sculpting in high-resolution nuclear magnetic resonance spectroscopy: application to selective NOE experiments. *J. Am. Chem. Soc.*, **117**, 4199–4200.
25. Orth,P., Saenger,W. and Hinrichs,W. (1999) Tetracycline-chelated Mg2+ ion initiates helix unwinding in Tet repressor induction. *Biochemistry*, **38**, 191–198.
26. Schumacher,M.A., Miller,M.C., Grkovic,S., Brown,M.H., Skurray,R.A. and Brennan,R.G. (2002) Structural basis for cooperative DNA binding by two dimers of the multidrug-binding protein QacR. *EMBO J.*, **21**, 1210–1218.
27. Miller,D.J., Zhang,Y.M., Subramanian,C., Rock,C.O. and White,S.W. (2010) Structural basis for the transcriptional regulation of membrane lipid homeostasis. *Nat. Struct. Mol. Biol.*, **17**, 971–975.
28. Orth,P., Schnappinger,D., Hillen,W., Saenger,W. and Hinrichs,W. (2000) Structural basis of gene regulation by the tetracycline inducible Tet repressor-operator system. *Nat. Struct. Biol.*, **7**, 215–219.
29. Itou,H., Watanabe,N., Yao,M., Shirakihara,Y. and Tanaka,I. (2010) Crystal structures of the multidrug binding repressor Corynebacteriumglutamicum CgmR in complex with inducers and with an operator. *J. Mol. Biol.*, **403**, 174–184.
30. Le,T.B., Schumacher,M.A., Lawson,D.M., Brennan,R.G. and Buttner,M.J. (2011) The crystal structure of the TetR family transcriptional repressor SimR bound to DNA and the role of a flexible N-terminal extension in minor groove binding. *Nucleic Acids Res*, 1–15.
31. Boehr,D.D., Nussinov,R. and Wright,P.E. (2009) The role of dynamic conformational ensembles in biomolecular recognition. *Nat. Chem. Biol.*, **5**, 789–796.
32. Pantoliano,M.W., Petrella,E.C., Kwasnoski,J.D., Lobanov,V.S., Myslik,J., Graf,E., Carver,T., Asel,E., Springer,B.A., Lane,P. *et al.* (2001) High-density miniaturized thermal shift assays as a general strategy for drug discovery. *J. Biomol. Screen.*, **6**, 429–440.
33. Niesen,F.H., Berglund,H. and Vedadi,M. (2007) The use of differential scanning fluorimetry to detect ligand interactions that promote protein stability. *Nat. Protoc.*, **2**, 2212–2221.
34. Reichheld,S.E., Yu,Z. and Davidson,A.R. (2009) The induction of folding cooperativity by ligand binding drives the allosteric response of tetracycline repressor. *Proc. Natl Acad. Sci. USA*, **106**, 22263–22268.
35. Han,B., Liu,Y., Ginzinger,S.W. and Wishart,D.S. (2011) SHIFTX2: significantly improved protein chemical shift prediction. *J. Biomol. NMR*, **50**, 43–57.
36. Pufall,M.A., Lee,G.M., Nelson,M.L., Kang,H.S., Velyvis,A., Kay,L.E., McIntosh,L.P. and Graves,B.J. (2005) Variable control of Ets-1 DNA binding by multiple phosphates in an unstructured region. *Science*, **309**, 142–145.
37. Yu,Z., Reichheld,S.E., Savchenko,A., Parkinson,J. and Davidson,A.R. A comprehensive analysis of structural and sequence conservation in the TetR family transcriptional regulators. *J. Mol. Biol.*, **400**, 847–864.
38. Le,T.B., Stevenson,C.E., Fiedler,H.P., Maxwell,A., Lawson,D.M. and Buttner,M.J. (2011) Structures of the TetR-like simocyclinone efflux pump repressor, SimR, and the mechanism of ligand-mediated derepression. *J. Mol. Biol.*, **408**, 40–56.
39. Hecht,B., Muller,G. and Hillen,W. (1993) Noninducible Tet repressor mutations map from the operator binding motif to the C terminus. *J. Bacteriol.*, **175**, 1206–1210.
40. Muller,G., Hecht,B., Helbl,V., Hinrichs,W., Saenger,W. and Hillen,W. (1995) Characterization of non-inducible Tet repressor mutants suggests conformational changes necessary for induction. *Nat. Struct. Biol.*, **2**, 693–703.
41. Urlinger,S., Baron,U., Thellmann,M., Hasan,M.T., Bujard,H. and Hillen,W. (2000) Exploring the sequence space for tetracycline-dependent transcriptional activators: novel mutations yield expanded range and sensitivity. *Proc. Natl Acad. Sci. USA*, **97**, 7963–7968.
42. Kamionka,A., Bogdanska-Urbaniak,J., Scholz,O. and Hillen,W. (2004) Two mutations in the tetracycline repressor change the inducer anhydrotetracycline to a corepressor. *Nucleic Acids Res.*, **32**, 842–847.
43. Scholz,O., Henssler,E.M., Bail,J., Schubert,P., Bogdanska-Urbaniak,J., Sopp,S., Reich,M., Wisshak,S., Kostner,M., Bertram,R. *et al.* (2004) Activity reversal of Tet repressor caused by single amino acid exchanges. *Mol. Microbiol.*, **53**, 777–789.
44. Gossen,M., Freundlieb,S., Bender,G., Muller,G., Hillen,W. and Bujard,H. (1995) Transcriptional activation by tetracyclines in mammalian cells. *Science*, **268**, 1766–1769.